The electronic properties of a homoleptic bisphosphine Cu(I) complex: a joint theoretical and experimental insight

Gianluca Accorsi,[a] Nicola Armaroli,[a] Béatrice Delavaux-Nicot,[b] Adrien Kaeser,[b] Michel Holler, [c] Jean-François Nierengarten[c] and Alessandra Degli Esposti[a,*]

† *Istituto per la Sintesi Organica e la Fotoreattività (ISOF), CNR, via P. Gobetti, 101, I-40129 Bologna, Italy*

‡ *Laboratoire de Chimie de Coordination du CNRS (UPR 8241), 205 route de Narbonne, 31077, Toulouse Cedex 4, France*

◇ *Laboratoir de Chimie des Matériaux Moléculaires, CNRS et Université de Strasbourg, Ecole Européenne de Chimie, Polymères et Matériaux, 25 rue Becquerel, 67087 Strasbourg Cedex 2, France*

* *E-mail: alessandra.degliesposti@isof.cnr.it*

Supplementary Data

Program References

· Gaussian 03, Revision D.02,

M. J. Frisch, G. W. Trucks, H. B. Schlegel, G. E. Scuseria, M. A. Robb, J. R. Cheeseman, J. A. Montgomery, Jr., T. Vreven, K. N. Kudin, J. C. Burant, J. M. Millam, S. S. Iyengar, J. Tomasi, V. Barone, B. Mennucci, M. Cossi, G. Scalmani, N. Rega, G. A. Petersson, H. Nakatsuji, M. Hada, M. Ehara, K. Toyota, R. Fukuda, J. Hasegawa, M. Ishida, T. Nakajima, Y. Honda, O. Kitao, H. Nakai, M. Klene, X. Li, J. E. Knox, H. P. Hratchian, J. B. Cross, V. Bakken, C. Adamo, J. Jaramillo, R. Gomperts, R. E. Stratmann, O. Yazyev, A. J. Austin, R. Cammi, C. Pomelli, J. W. Ochterski, P. Y. Ayala, K. Morokuma, G. A. Voth, P. Salvador, J. J. Dannenberg, V. G. Zakrzewski, S. Dapprich, A. D. Daniels, M. C. Strain, O. Farkas, D. K. Malick, A. D. Rabuck, K. Raghavachari, J. B. Foresman, J. V. Ortiz, Q. Cui, A. G. Baboul, S. Clifford, J. Cioslowski, B. B. Stefanov, G. Liu, A. Liashenko, P. Piskorz, I. Komaromi, R. L. Martin, D. J. Fox, T. Keith, M. A. Al-Laham, C. Y. Peng, A. Nanayakkara, M. Challacombe, P. M. W. Gill, B. Johnson, W. Chen, M. W. Wong, C. Gonzalez, and J. A. Pople, Gaussian, Inc., Wallingford CT, 2004.

· MOLDEN: G. Schaftenaar and J. H. Noordik, J. Comput.-Aided Mol. Design, 14 (2000) 123.

Reference for the X-Ray structure

O. Moudam, A. Kaeser, B. Delavaux-Nicot, C. Duhayon, M. Holler, G. Accorsi, N. Armaroli, I. Séguy, J. Navarro, P. Destruel, J.-F. Nierengarten, Chem. Commun. (2007) 3077.

Table S1: Comparison among the $^1S_0 \rightarrow ^1S_n$ excited state transitions calculated at the X-ray structure of $[Cu(dppb)_2]^+$ using different functionals with the 6-31+G(d) basis set and ECP10MWB(BAS2) or LANL8+(BAS3) psudopotentials and basis sets for Cu^+. Transition energies ΔE in eV, wavelengths λ in nm and oscillator strengths ($f_{osc.}$) are reported.

	PBE0/BAS2			B3LYP/BAS2			BMK/BAS2		
n	C_2	$\Delta E/\lambda$	$f_{osc.}$	C_2	$\Delta E/\lambda$	$f_{osc.}$	C_2	$\Delta E/\lambda$	$f_{osc.}$
1	A	3.79/327	0.0071	A	3.73/332	0.0056	A	4.11/302	0.0093
2	B	3.81/325	0.0526	B	3.75/330	0.0451	B	4.37/284	0.1120
3	B	3.99/311	0.0088	B	3.89/318	0.0077	A	4.44/279	0.0130
4	A	4.03/308	0.0002	A	3.92/316	0.0006	B	4.53/274	0.0239
5	A	4.11/301	0.0142	B	4.02/308	0.0290	B	4.59/270	0.0958
6	B	4.11/301	0.0400	A	4.02/308	0.0098	A	4.67/266	0.0917
	TPSS/BAS2			TPSS/BAS3			TPSSh/BAS3		
n	C_2	$\Delta E/\lambda$	$f_{osc.}$	C_2	$\Delta E/\lambda$	$f_{osc.}$	C_2	$\Delta E/\lambda$	$f_{osc.}$
1	A	3.10/400	0.0016	A	3.15/394	0.0020	A	3.51/353	0.0038
2	B	3.13/396	0.0325	B	3.17/390	0.0387	B	3.54/351	0.0433
3	B	3.19/388	0.0116	B	3.23/383	0.0131	B	3.62/342	0.0054
4	A	3.22/385	0.0032	A	3.26/381	0.0039	A	3.64/340	0.0022
5	A	3.39/366	0.0009	A	3.43/361	0.0015	A	3.81/325	0.0064
6	B	3.40/364	0.0746	B	3.45/360	0.0904	B	3.81/325	0.0292

Table S2: $^1S_0 \rightarrow ^1S_n$ excited state transitions of dppb calculated at its optimized geometry in solution using PBE0/6-31+G*. Transition energies ΔE in eV, wavelengths λ in nm and oscillator strengths ($f_{osc.}$) are reported.

n	$\Delta E/\lambda$	$f_{osc.}$	n	$\Delta E/\lambda$	$f_{osc.}$
1	4.0776/304	0.0523	20	5.4481/227	0.0229
2	4.0970/303	0.0626	21	5.4494/227	0.0401
3	4.2947/289	0.2118	22	5.4550/227	0.0224
4	4.5418/273	0.2252	23	5.4814/226	0.0077
5	4.6179/268	0.2869	24	5.5339/224	0.0010
6	4.6521/266	0.0487	25	5.5375/224	0.0010
7	4.7638/260	0.0034	26	5.5547/223	0.0470
8	4.8266/257	0.0029	27	5.5810/222	0.0117
9	4.8397/256	0.0447	28	5.5891/222	0.0003
10	4.9018/253	0.0131	29	5.5980/221	0.0009
11	4.9510/250	0.0008	30	5.6468/219	0.0027
12	5.0378/246	0.0205	31	5.6686/219	0.0067
13	5.1266/242	0.0027	32	5.6700/219	0.0029
14	5.1743/240	0.0016	33	5.6805/218	0.0005
15	5.2475/236	0.0006	34	5.7029/217	0.0191
16	5.3002/234	0.0195	35	5.7209/217	0.0479
17	5.3111/233	0.0126	36	5.7384/216	0.0506
18	5.3901/230	0.0140	37	5.7495/216	0.1468
19	5.3936/230	0.0155	38	5.7572/215	0.0134

Table S3: Calculated $^1S_0 \rightarrow ^1S_n$ transitions of $Cu[dppb]_2^+$ (C_2 symmetry) using PBE0/BAS1 at the geometry optimized considering solvation. h_n = HOMO - n and l_n = LUMO + n, ΔE (eV), λ (nm), and $f_{osc.}$(a.u.). The contributions by the two most significant excitations to each transition are indicated, with h_n = HOMO - n and l_n = LUMO + n.

n	C_2	$\Delta E/\lambda$	$f_{osc.}$	excitations
1	A	3.8534/322	0.0069	0.7h→l, -0.2h_1 →l_1
2	B	3.9651/313	0.1078	0.6h→l_1,-0.3h_1 →l
3	A	4.0902/303	0.0196	0.7h→l_2, -0.1h_1 →l_1,-0.1h_1 →l_3
4	B	4.1127/301	0.0116	0.5h_1 →l,0.3h→l_1,0.3h→l_3,-0.2h_1 →l_2
5	B	4.1814/296	0.0254	0.5h→l_3,-0.3h−1 →l_2,-0.3h−1 →l,0.2h→l_4,-0.2h→l_1
6	A	4.2491/292	0.0195	0.7h_1 →l_1,0.2h→l,0.1h→l_2
7	B	4.3276/286	0.1753	0.6h→l_4,0.2h_1 →l,0.1h_1 →l_2,0.1h_1 →l_5
8	B	4.3618/284	0.1495	0.6h_1 →l_2,0.4h→l_3
9	A	4.3840/283	0.1460	0.6h→l_5,0.2h_1 →l_4,0.1h_1 →l_3,0.1h→l_6
10	A	4.4455/279	0.0042	0.6h_1 →l_3, -0.2h→l_5, 0.1h→l_2, 0.1h→l_6
11	A	4.5320/274	0.0291	0.6h_1 →l_4,-0.3h→l_6,-0.2h→l_5
12	B	4.5626/272	0.0059	0.5h→l_7, 0.4h_1 →l_5,-0.3h_2 →l,0.1h_1 →l_8
13	A	4.5661/272	0.0089	-0.4h→l_6,0.4h→l_8,0.2h→l_5,0.2h_1 →l_7,0.1h_2 →l_1,0.1h_1 →l_1
14	B	4.6103/269	0.0222	0.6h_2 →l,0.3h_1 →l_5,0.2h→l_7
15	B	4.6325/268	0.0228	-0.4h_1 →l_5,0.4h→l_7,-0.2h_1 →l_6,0.2h_1 →l_8,0.1h_2 →l,0.1h→l_9,0.1h→l_4
16	A	4.6473/267	0.0001	0.5h→l_8,0.4h→l_6,0.2h_1 →l_4,0.1h_2 →l_1,0.1h_1 →l_7,-0.1h_1 →l_3
17	A	4.7381/262	0.0320	0.6h_2 →l_1,-0.2h→l_8
18	B	4.7544/261	0.1181	h_1 →l_6,h→h_9,h_1 →l_5,h_2 →l_2,h→l_7
19	B	4.8178/257	0.2005	-0.6h_2 →l_2,-0.1h_1 →l_6,0.1h→l_9
20	A	4.8360/256	0.0017	-0.6h→l_{10},-0.2h_1 →l_9,-0.1h_1 →l_7
21	B	4.8496/256	0.0198	0.4h→l_9,0.4h_1 →l_8,0.3h_1 →l_6,-0.1h→l_7
22	A	4.8540/255	0.0028	-0.6h_1 →l_7,0.2h→l_8,0.1h_2 →l_3,0.1h→l_{10}
23	B	4.8694/255	0.2079	-0.5h_1 →l_8,0.4h→l_9,0.1h_1 →l_6,0.1h→l_7
24	A	4.8828/254	0.0052	0.6h_2 →l_3,0.1h_1 →l_7
25	A	4.9408/251	0.0032	0.6h→l_{11},-0.2h_1 →l_9,-0.2h_1 →l_{12},0.1 h_2 →l_3,0.1h_2 →l_4,0.1h→l_{10}
26	B	4.9740/249	0.0189	0.5h_1 →l_{10},0.4h→l_{13},-0.2h→l_{15}
27	B	4.9769/249	0.0182	0.6h→l_{12},-0.2h_1 →l_{11},0.1h_2 →l_2

Table S4: Calculated $^1S_0 \rightarrow ^1S_n$ transitions of Cu[dppb]$_2^+$ in solution (C_2 symmetry) using PBE0/BAS1 at the geometry optimized *in vacuo*. h_n = HOMO - n and l_n = LUMO + n, ΔE (eV), λ (nm), and $f_{osc.}$(a.u.).

n	C_2	$\Delta E/\lambda$	$f_{osc.}$	n	C_2	$\Delta E/\lambda$	$f_{osc.}$
1	A	3.7087/334	0.0034	16	B	4.6696/266	0.0005
2	B	3.8701/320	0.0942	17	A	4.7268/262	0.0028
3	A	3.9606/313	0.0238	18	B	4.7294/262	0.1845
4	B	4.0293/308	0.0652	19	A	4.7920/259	0.0608
5	B	4.1129/301	0.0693	20	B	4.8478/256	0.0750
6	A	4.2078/295	0.0843	21	A	4.8572/255	0.0002
7	B	4.2781/290	0.1832	22	B	4.8595/255	0.0809
8	A	4.3877/282	0.0135	23	A	4.8941/253	0.0027
9	A	4.4492/279	0.0281	24	B	4.9027/253	0.0325
10	B	4.4508/278	0.0500	25	B	4.9294/252	0.0490
11	A	4.4947/276	0.0066	26	A	4.9422/251	0.0007
12	B	4.4965/276	0.0202	27	B	4.9573/250	0.0768
13	A	4.5421/273	0.0424	28	A	4.9622/250	0.0087
14	A	4.6332/268	0.0000	29	B	4.9866/249	0.1015
15	B	4.6356/267	0.0183	30	A	5.0038/248	0.0038

Table S5: Comparison among the calculated $^1S_0 \rightarrow ^1S_n$ transitions of $[Cu(dppb)_2]^+$ in solution [scrf=(cpcm,solvent=CH_2Cl_2)] and in the crystal. The symmetry labeling, the transition energies ΔE/eV, the wavelengths λ/nm and oscillator strengths ($f_{osc.}$) are reported.

	solution/BAS1			solution/BAS2			crystal/BAS2C		
n	C_2	$\Delta E/\lambda$	$f_{osc.}$	C_2	$\Delta E/\lambda$	$f_{osc.}$	C_2	$\Delta E/\lambda$	$f_{osc.}$
1	A	3.85/322	0.0069	A	3.78/328	0.0084	A	3.79/327	0.0071
2	B	3.97/313	0.1078	B	3.88/319	0.0908	B	3.81/325	0.0526
3	A	4.09/303	0.0196	A	4.03/308	0.0178	B	3.99/310	0.0088
4	B	4.11/301	0.0116	B	4.04/306	0.0139	A	4.03/307	0.0002
5	B	4.18/296	0.0254	B	4.11/301	0.0378	A	4.11/301	0.0142
6	A	4.25/292	0.0195	A	4.17/297	0.0175	B	4.11/301	0.0400
7	B	4.33/286	0.1753	B	4.24/292	0.1944	B	4.27/290	0.0835
8	B	4.36/284	0.1495	B	4.30/288	0.1199	A	4.27/290	0.0031
9	A	4.38/283	0.1460	A	4.30/288	0.1401	A	4.32/286	0.0624
10	A	4.45/279	0.0042	A	4.37/283	0.0041	B	4.33/286	0.0780
11	A	4.53/274	0.0291	A	4.45/278	0.0370	B	4.46/278	0.0154
12	B	4.56/272	0.0059	A	4.46/277	0.0002	A	4.48/276	0.0077
13	A	4.57/272	0.0089	B	4.48/276	0.0043	B	4.50/275	0.0403
14	B	4.61/269	0.0222	B	4.53/273	0.0292	A	4.54/273	0.0525
15	B	4.63/268	0.0228	B	4.55/272	0.0115	B	4.55/272	0.0255
16	A	4.65/267	0.0001	A	4.55/272	0.0012	A	4.60/269	0.0038

Table S6: Comparison among calculated $^1S_0 \rightarrow ^1S_n$ excited state transitions of $[Cu(dppb)_2]^+$ (PBE0/6-31G*) and $(dppb)_2$ (PBE0/6-31G*) at the optimized geometry of the complex in solution. Symmetry labels, transition energies ΔE/eV, wavelengths λ/nm and oscillator strengths ($f_{osc.}$) are reported.

	$[Cu(dppb)_2]^+$			$(dppb)_2$		
n	C_2	$\Delta E/\lambda$	$f_{osc.}$	C_2	$\Delta E/\lambda$	$f_{osc.}$
1	A	3.85/322	0.0069	A	3.46/358	0.0032
2	B	3.97/313	0.1078	B	3.49/355	0.0632
3	A	4.09/303	0.0196	A	3.70/335	0.0206
4	B	4.11/301	0.0116	B	3.70/335	0.0185
5	B	4.18/296	0.0254	B	3.81/326	0.0009
6	A	4.25/292	0.0195	A	3.83/324	0.0011
7	B	4.33/286	0.1753	B	3.89/319	0.0860
8	B	4.36/284	0.1495	A	3.90/318	0.1986
9	A	4.38/283	0.1460	B	4.02/309	0.0137
10	A	4.44/279	0.0042	A	4.02/308	0.0045
11	A	4.53/274	0.0291	B	4.05/306	0.0377
12	B	4.56/272	0.0059	A	4.05/306	0.0001
13	A	4.57/272	0.0089	B	4.09/303	0.0200
14	B	4.61/269	0.0222	A	4.15/299	0.0379
15	B	4.63/268	0.0228	B	4.17/297	0.0020
16	A	4.65/267	0.0001	A	4.17/297	0.0002
17	A	4.74/262	0.0320	B	4.25/292	0.0230
18	B	4.75/261	0.1181	A	4.30/288	0.0022
19	B	4.82/257	0.2005	A	4.31/288	0.0065
20	A	4.84/256	0.0017	B	4.32/287	0.2062
21	B	4.85/256	0.0198	A	4.34/286	0.0082
22	A	4.85/255	0.0028	B	4.36/284	0.0265
23	B	4.87/255	0.2079	A	4.37/284	0.0183
24	A	4.88/254	0.0052	B	4.38/283	0.2193

Table S7: Comparison among the calculated $^1S_0 \rightarrow {}^1S_n$ transitions of $Cu[dppb]_2^+$ at the X-ray geometry using PBE0 with (a) LANL8+ ECP and basis set for Cu^+, 6-31+G* for the other atoms, and (b) BAS2. h_n = HOMO - n and l_n = LUMO + n, ΔE (eV), λ (nm), and $f_{osc.}$(a.u.). The contributions by the two most significant excitations to each transition are indicated, with h_n = HOMO - n and l_n = LUMO + n.

	(a)				(b)			
n	C_2	$\Delta E/\lambda$	$f_{osc.}$	excitations	C_2	$\Delta E/\lambda$	$f_{osc.}$	excitations
1	A	3.86/321	0.0077	$0.64h_1 \rightarrow l$, $-0.26h \rightarrow l_1$	A	3.79/327	0.0071	$0.65h \rightarrow l$ $-0.26h_1 \rightarrow l_1$
2	B	3.88/319	0.0534	$0.61h \rightarrow l$, $-0.31h_1 \rightarrow l_1$	B	3.81/325	0.0526	$0.61h_1 \rightarrow l$ $-0.32h \rightarrow l_1$
3	B	4.06/305	0.0106	$0.59h_1 \rightarrow l_1$, $0.26h \rightarrow l$	B	3.99/311	0.0088	$0.59h \rightarrow l_1$ $+0.28$ $h_1 \rightarrow l$
4	A	4.09/303	0.0003	$0.61h \rightarrow l_1$, $0.25h_1 \rightarrow l$	A	4.03/308	0.0002	$0.63h_1 \rightarrow l_1$ $+0.24h \rightarrow l$
5	B	4.18/297	0.0342	$-0.45h_1 \rightarrow l_2$, $0.44h \rightarrow l_3$	A	4.11/301	0.0142	$0.51h_1 \rightarrow l_2$ $-0.43h \rightarrow l_3$
6	A	4.18/297	0.0145	$0.51h \rightarrow l_2$, $-0.42h_1 \rightarrow l_3$	B	4.11/301	0.0400	$0.47h \rightarrow l_2$ $-0.42h_1 \rightarrow l_3$
7	B	4.33/286	0.0845	$h_1 \rightarrow l_2$, $0.43h \rightarrow l_3$	B	4.27/290	0.0835	$0.45h_1 \rightarrow l_3$ $+0.45h \rightarrow l_2$
8	A	4.33/286	0.0040	$0.52h_1 \rightarrow l_3$, $0.45h \rightarrow l_2$	A	4.27/290	0.0031	$0.52h \rightarrow l_3$ $+0.45h_1 \rightarrow l_2$
9	A	4.38/283	0.0588	$0.65h \rightarrow l_4$, $0.21h_1 \rightarrow l_5$	A	4.32/287	0.0624	$0.64h_1 \rightarrow l_4$ $-0.22h \rightarrow l_5$
10	B	4.39/282	0.0786	$0.60h_1 \rightarrow l_4$,$-0.26h \rightarrow l_3$	B	4.33/286	0.0780	$0.61h \rightarrow l_4$ $-0.26h_1 \rightarrow l_3$
11	B	4.50/276	0.0204	$0.66h_2 \rightarrow l$	B	4.46/278	0.0154	$0.66h_2 \rightarrow l$
12	A	4.54/273	0.0067	$0.63h_1 \rightarrow l_5$,$-0.22h \rightarrow l_4$	A	4.50/277	0.0077	$0.64h \rightarrow l_5$ $+0.24h_1 \rightarrow l_4$

The MOs of dppb. The electron density plot of the frontier MOs of dppb (Figure S1). obtained by the PBE0/6-31+G(d) method, with the symmetry labeling referred to the C_s group, are shown in Figure S1. The HOMO and LUMO+1, calculated considering the molecule *in vacuo* at the geometry optimized with the symmetry constrains, are antisymmetric (A"), while the HOMO - 1 and LUMO are symmetric (A') with respect to σ_h reflection (xy plane). Most importantly, all these MOs are largely characterized by the lone pairs of the P atoms and all of them by the AOs of the central ring.

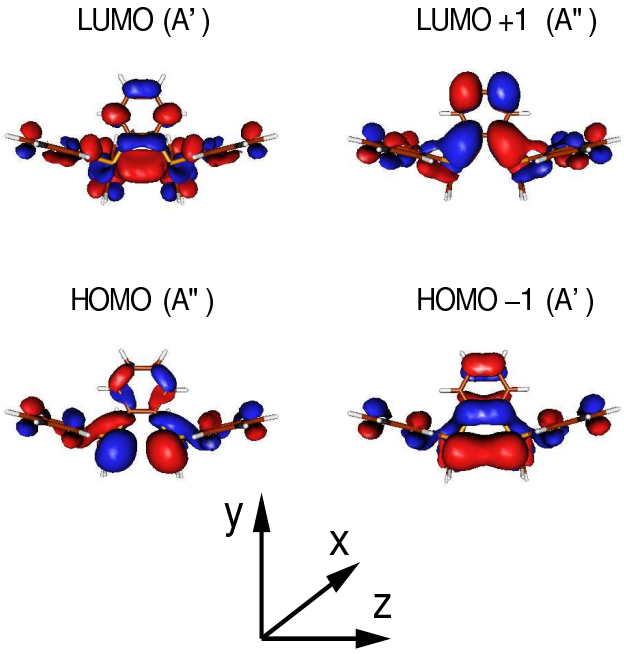

Figure S1: Calculated frontier MOs of dppb. The axes reference system is shown.

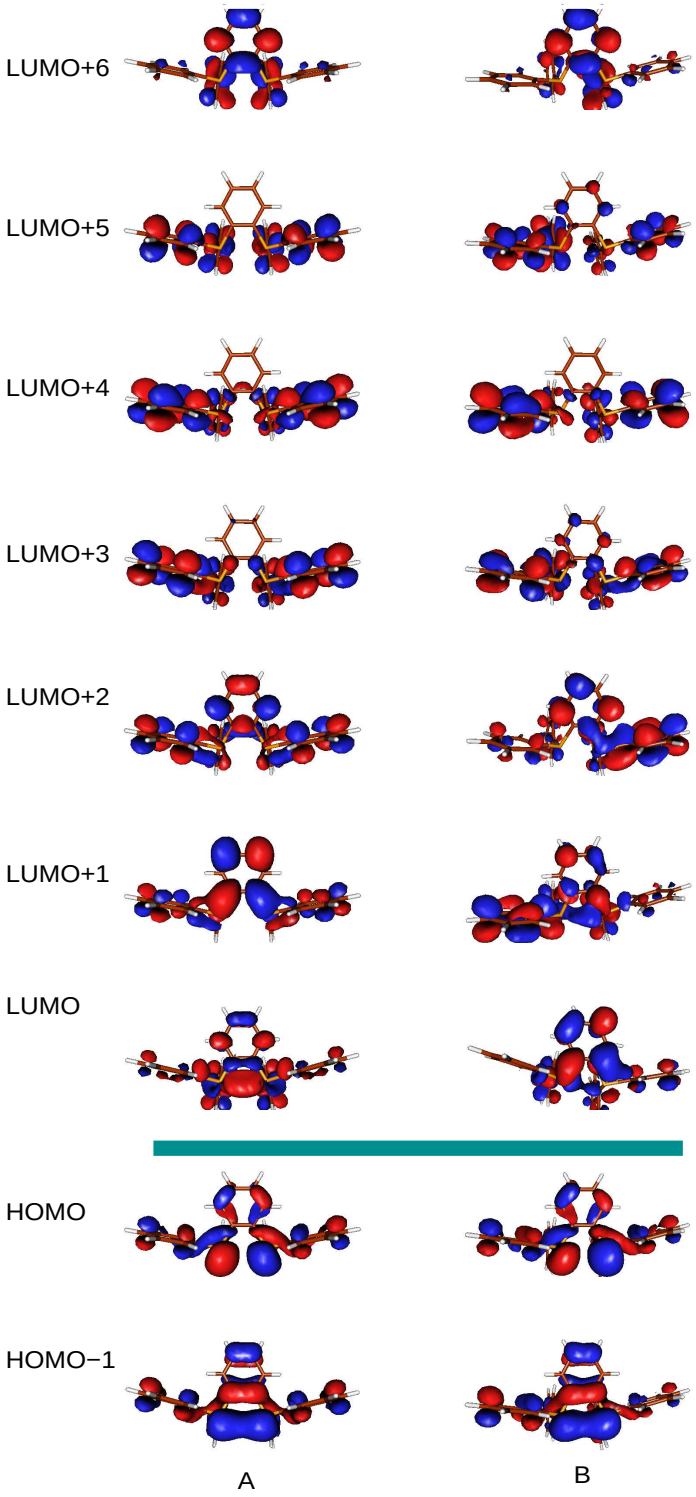

Figure S2: Comparison among the MOs of dppb calculated at the optimized geometries with C_s symmetry constraines (A) and at the structure assumed within the complex (B).

The MOs of $[Cu(dppb)_2]^+$. The $[Cu(dppb)_2]^+$ complex has the symmetry characteristics of the C_2 point group [Moudam *et al.*, Chem. Commun. (2007) 3077.], so that by rotation about the z axis, shown in Fig.2, the P_a and P_b atoms of one ligand (L_1) project into the P_a' and P_b' atomic positions of the other ligand (L_2), respectively. The analysis of the MOs, calculated by using the spherical harmonic description of the AOs (d^{m_l}, where m_l is the magnetic quantum number) evidences that all the $d^{0,\pm2}$ of Cu(I) contribute to the HOMO, while both the $d^{\pm1}$ contribute to the HOMO - 1 and HOMO - 2. Referring to cartesian coordinates, they correspond to d AOs with lobes oriented along the three molecular axes or lying on the xy plane (d_{z^2}, d_{x^2}-d_{y^2}, and d_{xy}) in the first case, or perpendicular to the xy plane (d_{xz}, and d_{yz}) in the second case. Besides, the contribution of the ligands to the HOMO and HOMO - 1 of the complex is described by an in-phase ($L^+ = L_1 + L_2$) and an out-of phase ($L^- = L_1 - L_2$) combination, respectively, of their HOMO (Figure S1), while the out-of phase (L^-) combination of the HOMO - 1 of the ligands with both the $3d^{\pm1}$ of Cu(I) characterizes the HOMO - 2 of the complex. The resulting shape of the density plots of these MOs are the bilobated banana-like HOMO and HOMO -1 shown in Fig.2, which connect the P_a (P_b) to the P'$_a$ (P'$_b$) and the P_a (P_b) to the P'$_b$ (P'$_a$) lone pairs of the two ligands, respectively, or the P_a (P'$_a$) to the P_b (P'$_b$) of the same ligand in the case of the HOMO - 2 of the complex (Figure S3). Moreover, the HOMO of $[Cu(dppb)_2]^+$ transforms by a rotation of π angle about the z axis as the A irreducible representation, while both the HOMO - 1 and HOMO - 2 as the B irreducible representations of the C_2 symmetry group. The lower lying unoccupied MO can be correlated with the antisymmetric LUMO + 1 of dppb (Figure S1) since within the complex the aryl substituents of the ligands do not preserve locally the C_s symmetry. Within C_2 symmetry, LUMO and LUMO + 1 of the complex transform as the A and B irreducible representations, respectively. The low energy LUMO + n (Figure S3) are largely characterized by the central phenyl unit while the contribution by the other aryls increases at higher energy, as in the case of the ligands alone.

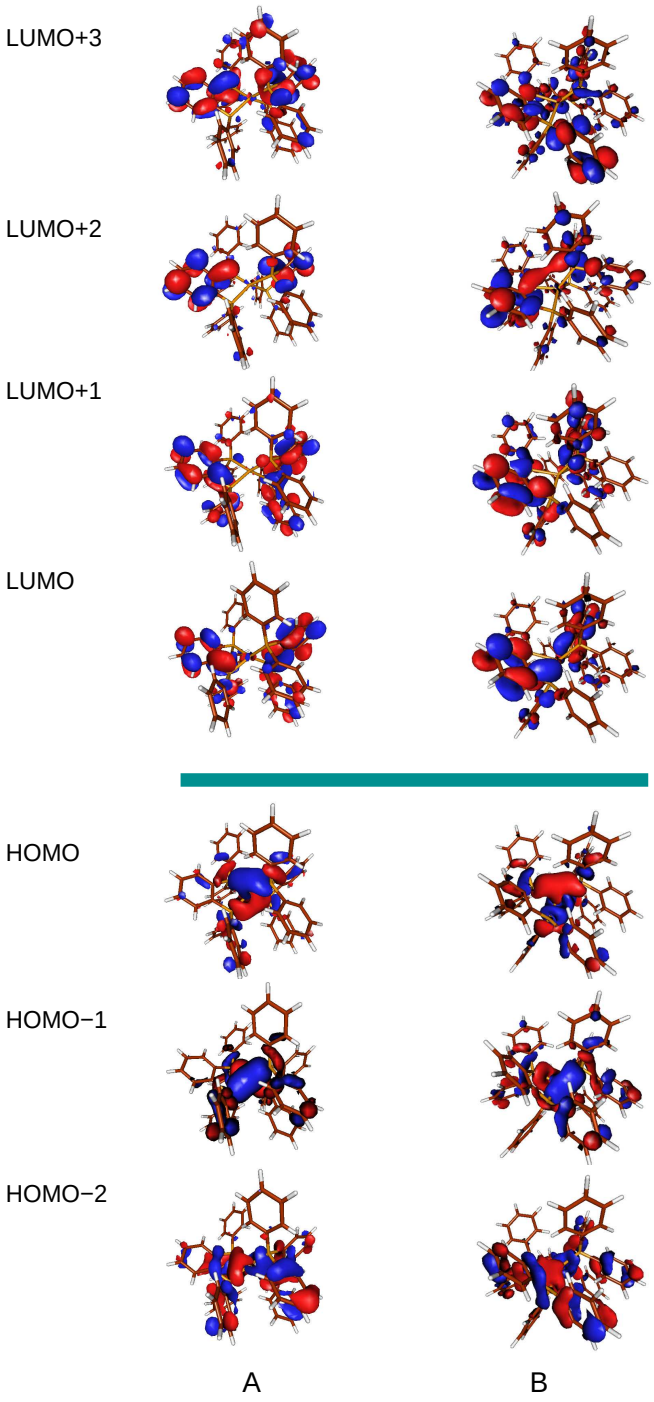

Figure S3: Comparison among the MOs of $[Cu(dppb)_2]^+$ calculated (A) at its X-ray stucture and (B) at its calculated geometry *in vacuo*.